

# Findings from the Supersonic Qualification Program of the Mars Science Laboratory Parachute System

Anita Sengupta<sup>\*</sup>, Adam Steltzner<sup>†</sup>  
*Jet Propulsion Laboratory, California Institute of Technology, Pasadena, CA,*

Allen Witkowski<sup>‡</sup>  
*Pioneer Aerospace, South Windsor, CT*

Graham Candler<sup>§</sup>  
*University of Minnesota, Minneapolis, MN*

Carlos Pantano<sup>\*\*</sup>  
*University of Illinois, Urbana-Champaign, IL*

In 2012, the Mars Science Laboratory Mission (*MSL*) will deploy *NASA*'s largest extra-terrestrial parachute, a technology integral to the safe landing of its advanced robotic explorer on the surface. The supersonic parachute system is a mortar deployed 21.5 m disk-gap-band (*DGB*) parachute, identical in geometric scaling to the Viking era *DGB* parachutes of the 1970's. The *MSL* parachute deployment conditions are Mach 2.3 at a dynamic pressure of 750 Pa. The Viking Balloon Launched Decelerator Test (*BLDT*) successfully demonstrated a maximum of 700 Pa at Mach 2.2 for a 16.1 m *DGB* parachute in its AV4 flight. All previous Mars deployments have derived their supersonic qualification from the Viking *BLDT* test series, preventing the need for full scale high altitude supersonic testing. The qualification programs for Mars Pathfinder, Mars Exploration Rover, and Phoenix Scout Missions were all limited to subsonic structural qualification, with supersonic performance and survivability bounded by the *BLDT* qualification. The *MSL* parachute, at the edge of the supersonic heritage deployment space and 33% larger than the Viking parachute, accepts a certain degree of risk without addressing the supersonic environment in which it will deploy. In addition, *MSL* will spend up to 10 seconds above Mach 1.5, an aerodynamic regime that is associated with a known parachute instability characterized by significant canopy projected area fluctuation and dynamic drag variation. This aerodynamic instability, referred to as "area oscillations" by the parachute community has drag performance, inflation stability, and structural implications, introducing risk to mission success if not quantified for the *MSL* parachute system. To minimize this risk and as an alternative to a prohibitively expensive high altitude test program, a multi-phase qualification program using computation simulation validated by subscale test was developed and implemented for *MSL*. The first phase consisted of 2% of full-scale supersonic wind tunnel testing of a rigid *DGB* parachute with entry-vehicle to validate two high fidelity computational fluid dynamics (*CFD*) tools. The computer codes utilized Large Eddy Simulation and Detached Eddy Simulation numerical approaches to accurately capture the turbulent wake of the entry vehicle and its coupling to the parachute bow-shock. The second phase was the development of fluid structure interaction (*FSI*) computational tools to predict parachute response to the supersonic flow field. The *FSI* development included the integration of the *CFD* from the first phase with a finite element structural model of the parachute membrane and cable elements. In this phase, a 4% of full-scale supersonic flexible parachute test program was conducted to provide validation data to the *FSI* code and an empirical dataset of the *MSL* parachute in a flight-like environment. The final phase is *FSI* simulations of the full-scale *MSL* parachute in a Mars type deployment. Findings from this program will be presented in terms of code development and validation, empirical findings from the supersonic testing, and drag performance during supersonic operation.

---

<sup>\*</sup> Senior Engineer, *EDL* and Advanced Technologies, 4800 Oak Grove Dr, MS 301-440C, Senior Member AIAA.

<sup>†</sup> Program Manager, *EDL* and Advanced Technologies, 4800 Oak Grove Dr, T1723-118, Senior Member AIAA.

<sup>‡</sup> Director Engineering Operations, 45 S. Satellite Rd., Member AIAA.

<sup>§</sup> Professor, Dept. of Aerospace Engineering, 107 Akerman Hall, 110 Union St SE, Fellow, AIAA.

<sup>\*\*</sup> Asst. Professor, Dept. of Mechanical Science and Engineering, 1206 West Green Street, MC-244, Member AIAA.

## Nomenclature

$d$	=	Capsule diameter
$D_o$	=	Parachute nominal diameter
$x/d$	=	Non-dimensional trailing distance measured from capsule to parachute band leading edge
$Re$	=	Reynolds number
$DGB$	=	Disk Gap band
$FSI$	=	Fluid Structure Interaction
$CFD$	=	Computational Fluid Dynamics
$BLDT$	=	Balloon Launched Decelerator Test
$PEPP$	=	Planetary Entry Parachute Program
$MER$	=	Mars Exploration Rover
$MPF$	=	Mars Pathfinder
$SHAPE$	=	Supersonic High Altitude Parachute Experiment
$PDS$	=	Parachute Decelerator System
$RCS$	=	Reaction Control System
$RCS$	=	Root Mean Squared

## I. Introduction

The Mars Science Laboratory (*MSL*) is *NASA's* next landed mission to the planet Mars. The mission will deliver to the surface *NASA's* most capable robotic geologist, a 900 kg laboratory equipped with an instrument suite to analyze the atmosphere and soil searching for carbon-based molecules and water, the building blocks of life. The science objectives of the mission necessitate access to landing sites that are characterized by up to 2 km above the gravitational equi-potential reference surface, 60 degrees from the equator, and a challenging surface terrain<sup>1</sup>. These sites have previously been inaccessible due to limitations in the precision and capability of the Entry Descent and Landing (*EDL*) system/phase of the Mars Exploration Rover, Phoenix, and Mars Pathfinder missions<sup>2</sup>. The *EDL* phase of *MSL* is uniquely equipped, however, to meet these landing site challenges with a lifting-body trajectory from hypersonic entry to parachute deploy, active *RCS* control throughout the *EDL* sequence, a supersonic parachute, propulsive descent, and a tethered touchdown maneuver<sup>3</sup>, yielding an error ellipse of 10 km from the designated surface target<sup>4,5</sup>.

The parachute is a critical element of all Mars *EDL* systems providing a mass and volume efficient source of aerodynamic drag. The parachute also provides the required difference in ballistic coefficients during the heat-shield and descent-vehicle separation events. During terminal descent, the parachute places the descent-vehicle (containing the Rover) at the appropriate velocity and altitude for a final propulsive descent to the surface. The *MSL* parachute is based on the Viking heritage disk-gap-band design (*DGB*), originally developed in the 1970's to maximize drag and stability at supersonic speeds in low dynamic pressure environments<sup>6</sup>. The Viking program qualified a 16.1-m nominal diameter *DGB* parachute over a range of supersonic, low-dynamic-pressure deployments through a series of high altitude balloon-launched rocket-assisted flight tests<sup>7,8</sup>. The Viking Balloon Launched Decelerator Test (*BLDT*) essentially qualified the *DGB* parachute design for deployments up to 700 Pa and Mach 2.2<sup>9</sup>. All *NASA* Mars missions since the Viking Lander have flown *DGB's* less than 16 m in diameter and deployed at less than Mach 2, enabling them to take advantage of the existing supersonic qualification and eliminate the need for a prohibitively expensive high altitude test program<sup>10</sup>. *MSL* presents a departure from the existing heritage argument however, as it will fly a 21.5-m *DGB* and deploy at up to 750 Pa and Mach 2.3, making it the largest, fastest, and highest opening load *DGB* parachute ever to be deployed on Mars (or Earth).

The aforementioned *MSL* parachute size and deployment conditions were selected to provide the drag, ballistic coefficient and terminal velocity to achieve the *EDL* timeline and to provide geometric, aerodynamic, and trajectory

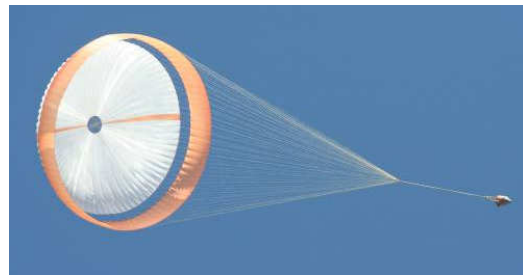


**Fig 1. Full-scale *MSL* parachute tested subsonically on Earth.**

similarity to the Viking *BLDT* qualification flights<sup>8</sup>. However this trajectory will subject the parachute to up to 10 seconds of operation above Mach 1.5. This is an area of concern as *DGB* parachutes tested supersonically from the Viking and pre-Viking era have been observed to exhibit a supersonic instability between Mach 1.5 and 2.5<sup>11,12,13</sup>. The instability is characterized by periodic in-folds in the band, leading to localized fabric collapse and subsequent re-inflation. Each re-inflation event subjects the parachute to a load on the order of the opening load. This phenomenon is commonly referred to as “area oscillations” and results in unsteady drag coincident with shape and lateral instability. For the past several decades this phenomenon has been attributed to aero-elastic effects of the suspension lines, fabric porosity, and entry-vehicle wake interaction at high Mach numbers. However, the exact source of the phenomenon was unknown requiring a study specific to determining its cause for the *MSL* parachute implementation.

The *MSL* concern with area oscillations includes uncertainties in the modeling of the descent-phase of the mission (parachute drag and stability), difficulty in quantifying the parachute’s dynamic loading, and impact on the parachute’s structural integrity due to self-abrasion and repeated loading events. Although from a non-dimensional aerodynamic parameter perspective *MSL* falls within the heritage deployment space, the larger size in conjunction with a Mach 2.3 deployment brought with it the possibility of a scale-dependent dynamic response to area oscillations that is not represented by the Viking *BLDT* 16.1-m flight-test data. In the absence of a prohibitively expensive full-scale supersonic test, an analytical understanding of the scale-dependent, aero-structural response was required to extrapolate the inflation, drag, stability and structural performance of the *MSL* parachute from the Viking *BLDT* database. Unlike the prior Mars Missions since Viking (MPF, MER, and Phoenix) a supersonic qualification program was implemented for *MSL*.

Three years later, through a combination of subscale supersonic wind tunnel tests and validated computational fluid dynamics and fluid structure interaction simulations, physical insight into the scale, material, and aerodynamic dependence of supersonic *DGB* parachute operation has been ascertained. This approach has mitigated the risk associated with the large scale and high Mach deployment of *MSL*. It has also provided a framework for future design by analysis and subscale test that is needed as payload requirements increase on our path toward manned exploration of Mars. The discussion of this program’s findings will be presented in this article.

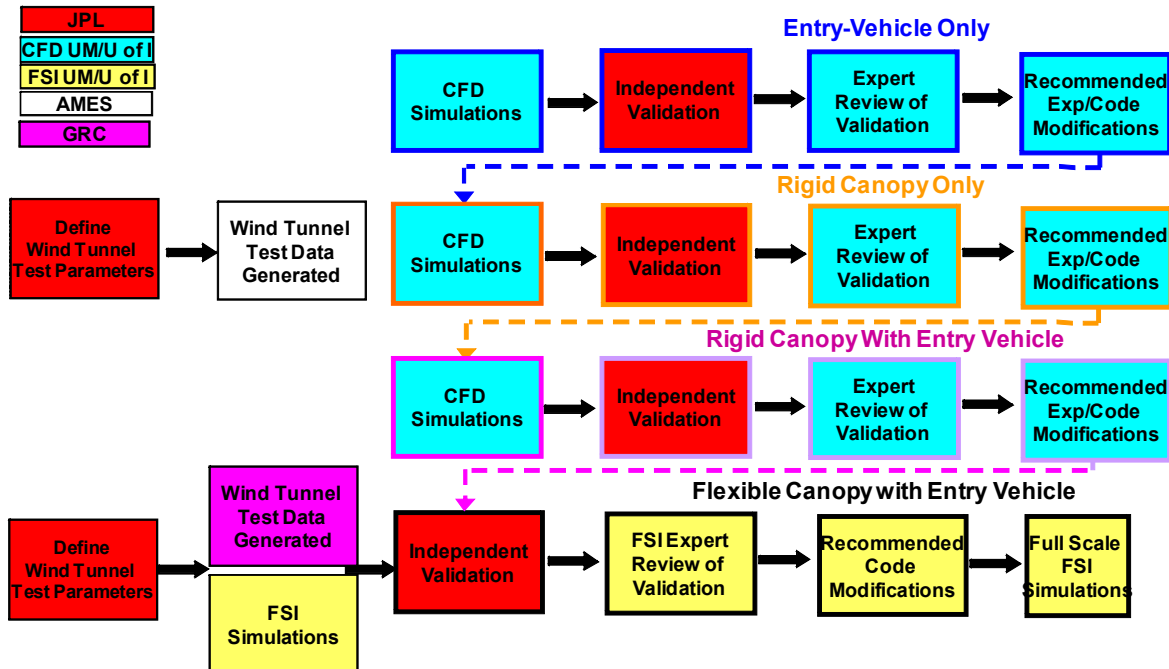


Fig 2. *MSL* supersonic qualification by computational simulation and subscale test process diagram.

## II. Supersonic Qualification Process

Use of computational simulations for qualification requires both qualitative and quantification validation to ensure accuracy and applicability to the problem of interest. To garner an understanding of the flow field and ensure the

validity of the simulations, a multi-phase experimental test program and with simulation validation process were developed as shown in Fig. 2. The validation process had 4 phases. The first three phases were associated with a “Rigid Parachute” experiment, intended to explore the fundamental physics of the entry-vehicle wake, blunt body flow around the parachute, and the coupling of the two at supersonic speeds<sup>26</sup>. The test and simulation matrix was designed to explore the effects of Mach, Reynolds number, parachute size, trailing distance. Phase 4 was a flexible parachute experiment with corresponding *FSI* simulations. The flexible parachute experiment was intended to explore the fabric response to the aerodynamic environment, specifically looking at quantifying the area oscillation instability in terms of drag performance, stability, and repeated loading as a function of Mach, Re, dynamic pressure, parachute trim angle, and parachute material properties. The design of experiments for each test program was conducted with the aid of *CFD/FSI* including test article mounting considerations and aerodynamic disturbance, test scaling, diagnostic selection, and grid-ability of all hardware to be used. The validation process had inherent in it peer review of each dataset and the possibility for modification to either the code or experiment following each phase, as needed. At the conclusion of the process an assessment of the supersonic parachute will be made in the context of the Viking *BLDT* existing qualification and the applicability of extrapolation from it.

### III. Computational Tool Development

#### A. CFD Development

The first phase of the supersonic qualification program was the conduct of *CFD* validation simulations of a 2% scale rigid *MSL* parachute with entry-vehicle experiment. The limitation of *CFD* with regard to the parachute problem is that a rigid representation of the parachute is required in addition to a fixed location with respect to the entry-vehicle for a given run. In spite of this, *CFD* predictions can provide detailed physical insight into the flow field parameters including the effect on canopy pressure distribution, turbulent wake structure, geometric scaling and alignment, and therefore the resultant interaction of the turbulent wake of the entry-vehicle with the parachute blunt body, in supersonic flow. The rigid parachute experiment will be discussed further in section IV.

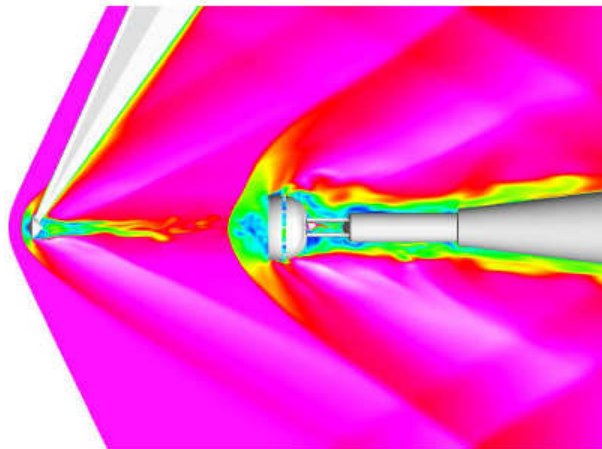


Fig 3. Rigid parachute and capsule wake *DES* simulation from the University of Minnesota<sup>30</sup>.

Two *CFD* codes were developed for the *MSL* supersonic parachute qualification program. *US3D*, an unstructured grid Detached Eddy Simulation (*DES*) solver was developed by the University of Minnesota to handle the turbulent, unsteady, and highly separated flow characteristics of the parachute wake interaction problem<sup>14,15,16</sup>. Figure 3 is a *US3D* simulation where the instantaneous turbulent flow structures in the wake are evident in the computation.. The second code is the Virtual Test Facility (*VTF*), originally developed at the California Institute of Technology for the Advanced Simulation and Computing (*ASC*) program for the Department of Energy<sup>17,18</sup>. The code has been under development for the simulation of parachutes at the University of Illinois in support of the *MSL* program. *VTF* is a *CFD/FEM* toolkit. The *CFD* solver is a fully adaptive Large Eddy Simulation (*LES*) with adaptive mesh refinement (*AMR*) enabling highly accurate computation of turbulence, separation, shock capturing, and moving geometries<sup>19</sup>. Figure 4 is a simulation of an *FSI* simulation with the *VTF*. The validation of both codes is discussed in section IV.

Validation simulations using *US3D* and *VTF* were run for the sub-scale rigid parachute wind tunnel experiments. The simulations indicate a highly turbulent wake from the entry-vehicle with a range of vortex shedding frequencies and a helical instability mode. The subsonic wake structure bleeds into the canopy, resulting in a pressurization and depressurization of the canopy coincident with a change in the bow-shock between conical and normal in a cyclical manner. The periodic pressurization manifests as a bow-shock oscillation and highly unsteady drag force. The phenomenon is found to depend on relative wake size, proximity to the parachute, Reynolds number, and Mach number, consistent with the experimental results of the rigid test program (to be discussed in section IV). At Mach 1.5 the parachute bow-shock is detached and exhibited less coupling to the wake. At Mach 2.5 the coupling was significant as was the resultant drag variation. Predictions of canopy pressure

distribution, also indicate fluctuations in the band region, with a more uniform loading in the disk region, suggesting that the area oscillation is driven by band fluctuations consistent with prior flight tests and the *MSL* flexible parachute experiment<sup>7, 8, 31, 32</sup>.

## B. FSI Development

The second phase of the computational effort was fluid structure interaction (*FSI*) code development and validation with a subscale flexible parachute wind tunnel test (section V). *FSI* refers to the interaction of the flow field on the flexible parachute and vice versa. *FSI* simulation provides prediction of parachute drag, stability, and transient loading as a result of the canopy's response to the flow field. Once validated, an *FSI* code can be used to predict the performance of the full scale parachute including material property dependencies. Due to their small size, suspension lines can only be modeled at cable elements permitting response to the flow field but no aerodynamic effect on it. The real challenge associated with *FSI* in highly separated supersonic flow is the capability to restructure the fluid grid in time as the parachute translates and collapses in response to the aerodynamic forces.

As with the *CFD* solvers two *FSI* tools were developed. *US3D* was coupled with a Lagrangian membrane element based Finite Element Model (*FEM*) from the US Army Natick<sup>20,21</sup>. The parachute was modeled as a zero thickness membrane with cable elements for the suspension lines and radial reinforcements. *CFD* grid re-computation was accomplished by grid distortion to reflect the new position of the canopy as a result of its interaction with the flow field. The *CFD* solver provides normal and shear forces to the structural solver and the membrane and *CFD* grid is moved or distorted accordingly. The *VTF* was modified to allow coupling between the existing *LES* and *FEM* modules. The parachute was modeled with thin shelled elements, a more accurate way to represent fabric motion as it provides for resistance to bending needed to capture wrinkling and other larger deformations of the parachute fabric<sup>22</sup>. The *FEM* mesh is computed by interpolation of shape functions based on minimizing the energy of the membrane in the newly deformed configuration<sup>23</sup>. AMR enables dynamic adaptation of the fluid mesh to better resolve the flow features of interest in response to the deforming parachute. Coupling of the *CFD* and *FEM* solvers is accomplished by the Ghost Fluid Method and Close-Point-Transformation algorithm<sup>24</sup>.

## IV. Rigid Parachute Experiment

A 2% of flight scale rigid *DGB* parachute with scaled entry-vehicle was tested in the *NASA* Ames 9'x7' (2.1 x 2.7 x 12.1 m test section) and *NASA* GRC 10'x10' (3m x 3m x 12.2m test section) supersonic wind tunnels over a range of Mach 1.5 to 2.5 and Reynolds number of  $7 \times 10^5$  and  $5 \times 10^6$ , bounding all possible *MSL* deployment conditions<sup>††</sup>. Both facilities are closed loop, variable pressure (to simulate Mars pressure), and operate on standard air. The test program explored three fundamental configurations: entry-vehicle alone, canopy alone, and entry-vehicle with canopy, providing a piecewise understanding of the flow field and the resultant fluid structure

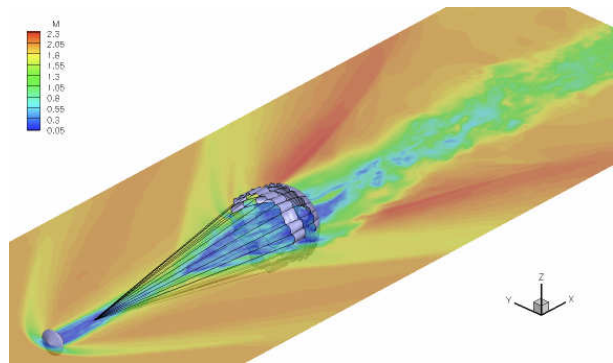


**Fig 4. Flexible parachute with entry vehicle LES simulation from the University of Illinois.**

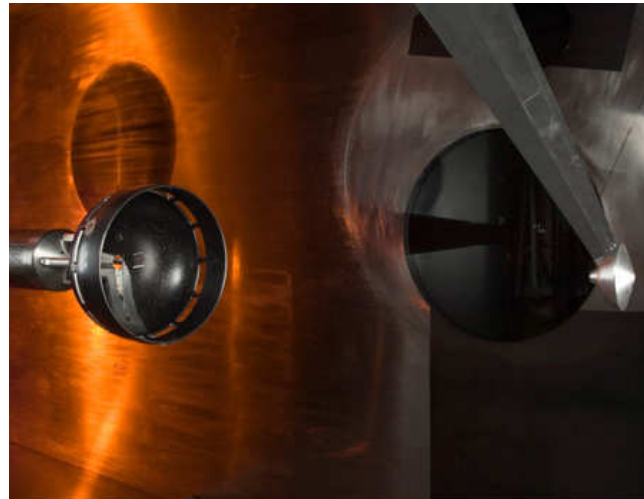


**Fig 5. (Left) *MSL* 2% scale rigid parachute test in the GRC 10x10 supersonic wind tunnel. (Right) Capsule wake PIV measurement from the 10x10 experiment.**

<sup>††</sup> The rigid experiment was conducted in two facilities due to facility availability and to investigate facility induced effects (none were observed). Canopy alone runs were only performed in the Ames 9x7 facility.

**Table 1. Rigid canopy-with-capsule experiment test matrix<sup>26</sup>.**

Test Configuration	Mach Number ( $M_\infty$ )	Parachute Trim Angle (deg)	Capsule AOA (deg)	$d/D_o$	$D_o$ [m] (Flight Equivalent)	Test Facility	$x/d$
Capsule Only	1.5,2,2.5 2,2,2.5	---	0, 5, 0,10	---	---	9x7 10x10	---
Canopy Only	1.5,2,2.5	0, 5, 10	0	---	---	9x7	---
19.7-m Canopy with Capsule	1.5,2,2.5	0, 5, 10	0	0.23	19.7	9x7	10
	1.5,2,2.5	0, 5, 10	5	0.23	19.7	9x7	10
		0	0	0.23	19.7	9.7	14
		0	0	0.23	19.7	10x10	9.9
23-m Canopy with Capsule	2,2,2,2.5	0, 5, 10	0	0.2	23	10x10	11.7
25-m Canopy with Capsule	2,2,2,2.5	0	0, 10	0.18	25	10x10	10

interaction. The rigid test also investigated the effects of parachute size, parachute trim angle, entry vehicle angle of attack, and trailing distance between the entry-vehicle and canopy. The detailed test matrix is shown in Table 1.

*CFD* was used in the design of the test configuration, a necessity for a validation experiment. Specifically, simulations were performed to ensure that all test article mounting fixtures would not significantly alter the physics of interest, i.e. entry-vehicle wake and its interaction with the canopy bow-shock<sup>19</sup>. Computational grid-generation considerations were used to refine the mounting fixture design and fabrication processes (i.e. edge effects). *CFD* was also used to size fixtures to ensure adequate canopy apex venting and that all major shocks would reflect downstream of the parachute. Computational experts were also consulted in the selection of diagnostics and data plane locations to maximize the experimental data output validation potential.

### A. Test Article and Configuration

The test configuration is shown in Fig.5 indicating the rigid parachute and entry vehicle mounting arrangement. A 0.457 m nominal diameter ( $D_o$ ) canopy and 0.104 m maximum diameter ( $d$ ) entry vehicle (2% of full scale) were selected to ensure that the entry-vehicle bow-shock reflected downstream of the canopy in the 9x7 test section, the smaller of the two test facilities. The rigid canopy shape represents the mean inflated shape of the full scale parachute during the nominal Mars supersonic deployment. The finite element membrane solver *TENSION* was used to compute the full-scale parachute shape with a uniform pressure distribution applied in the interior and appropriate material properties and construction techniques for each gore, reinforcements, and suspension lines<sup>20</sup>. The rigid canopy was made from an aluminum disk and connected to a steel band via twelve evenly spaced aluminum struts, to represent the gap. Considerable analysis (and test) went into the design of the rigid canopy to ensure that natural modes of the canopy, aerodynamic environment, and general tunnel operation did not couple. The canopy was mounted to a 6-axis force balance at the apex via 4 struts and balance block mount. The length of the struts was selected to ensure adequate venting from the canopy apex (as computed by *CFD*). The strut geometry was chosen to minimize thickness but ensure sufficiently structural integrity to ensure a truly rigid canopy. The canopy was 5 mm thick, selected to provide structural integrity but minimize edge effects from the blunt cross section. The entry-vehicle model was directly scaled from the flight outer-mold line and milled from a solid piece of aluminum. To investigate the effect of parachute size, three different capsule sizes were built to simulate  $d/D_o$  ratios for a 19.7, 23, and 25 m parachute. To investigate the effect of entry-vehicle angle of attack relative to the free stream, three separate capsules were built to simulate 0, 5, and 10 degrees relative to the free stream. The capsule was fitted with two penetrations for the two Kulites transducers. The tunnel to entry-vehicle mounting was achieved with a 45-deg swept diamond-edge sting, similar in design to that used by the Viking era subscale wind tunnel programs<sup>25</sup>. The sting cross section and leading edge shape were designed to provide minimum flow disturbance, sufficient stiffness to prevent capsule vibration, and be grid-able by the *CFD* solvers. A maximum deflection of 0.1 deg was selected as the required stiffness criteria. Trailing distance ( $x/d$ ) variation was accomplished via movement of the strut attachment to the tunnel ceiling upstream or downstream, providing a range of 10 to 14. The canopy and force balance was mounted to a high precision translation stage allowing this movement in precise intervals during a tunnel run. Parachute trim angle variation was therefore approximated via translation of the rigid canopy in the cross-stream direction<sup>26</sup>.

## B. Diagnostics

The diagnostic approaches selected were intended to be non-intrusive, yet provide spatial and temporal resolution of the flow field and parachute's response to it. High speed Kulites transducers were used to measure pressure on the entry vehicle surface and in the canopy interior. A 6-component strain-gauge balance (2.5-in MK16) was mounted to the canopy apex providing time resolved measurements of normal and transverse forces and moments<sup>27</sup>. Pressure and force data were collected at 10 kHz. Shadowgraph imaging of the canopy bow-shock was captured by a high speed camera at a frame rate of 3 kHz in the 9x7 facility. In the 10x10 facility, Schlieren imaging of the bow-shock was obtained with a high speed camera at 4 kHz frame rate. Comparison of the two techniques indicated that Shadowgraph provided optimum resolution of the bow-shock, the measurement of interest for code validation purposes. As a result Shadowgraph was selected for the flexible parachute experiment (Section V). The most complex but highest value diagnostic technique selected was particle image velocimetry (*PIV*). *PIV* provides a non-intrusive means to obtain time accurate measurements of the three components of velocity in a two-dimensional (2D) data plane with high spatial resolution ( $\sim 2$  mm). *PIV* provides an excellent measure of unsteady flow, including instantaneous velocity vectors, mean and *RMS* velocity, and turbulent statistics, enabling direct comparison to *CFD* prediction for validation purposes. Three *PIV* data planes were investigated for the rigid parachute experiments: (1) an entry vehicle alone cross-stream plane at  $x/d=10$  to measure radial wake expansion (9x7 facility), (2) a stream-wise plane with an axial extent from  $x/d=2$  to 6 for wake closure measurements (9x7 facility), and (3) a stream-wise plane from  $x/d=8$  to 10 (10x10 facility) to measure the velocity distribution in parachute bow-shock region. The *PIV* has an accuracy of 3% for each instantaneous velocity measurement and 1% for mean velocity measurements. More details on the *PIV* technique and implementation in the two test facilities can be found in references 19 and 28.

## C. Entry Vehicle Alone Results

*PIV* measurements of mean axial velocity from the entry vehicle alone configuration are shown in Fig. 6 and 7. The *PIV* data also measure the unsteadiness of the flow field (turbulence statistics) and the effect of the sting on the wake structure. Figure 6 is an image of the radial variation of the wake, which indicates an oblong structure, the effect of the sting on the wake structure. The measured wake deficit region was  $\sim 0.2$  m radially from the centerline at the  $x/d=10$  location. Figure 7 is an image of the axial extent of the wake closure region. The wake was found to recover to supersonic speeds at 0.3 m downstream of the entry-vehicle at Mach 2.0. Figure 8 is a comparison of the measured and simulated *RMS* axial velocity component at the  $x/d=10$  location at Mach 2.0. Comparison of the mean axial velocity in the deficit region compared to within 3% for mean values and 10% for *RMS*. This indicates good agreement with the energy content and unsteadiness of the flow field.

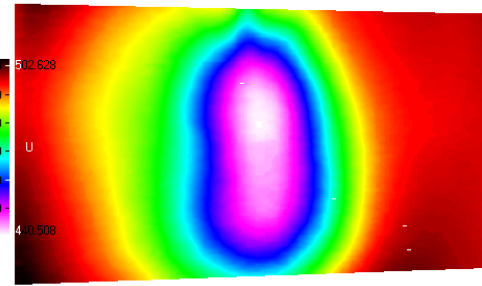
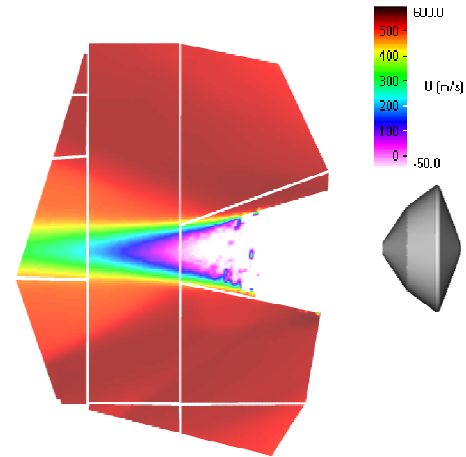


**Fig 6. Ames 9x7 test entry-vehicle alone axial velocity *PIV* data for (top) the axial plane from  $x/d=2$  to 6 and (bottom) the radial plane at  $x/d=10$  for Mach 2.0<sup>19</sup>.**

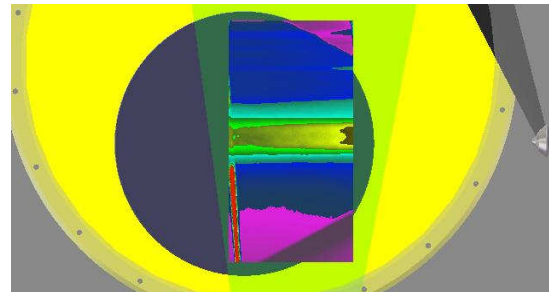


**Fig 7. GRC 10x10 *PIV* data at Mach 2 for (left) test entry-vehicle alone and (right) entry-vehicle with canopy from an axial plane from  $x/d=2$  to 6 for Mach 2.0<sup>28</sup>.**

#### D. Canopy Alone Results

Figure 9 (top) is a shadowgraph of the canopy alone flow field at Mach 2.0. In this configuration both the sting and capsule were removed from the test chamber. The bow-shock was observed to be steady, symmetric, and detached from Mach 1.5 to 2.5. Similarly the drag was steady with a minimal *RMS* component. The experimental results indicate that without a capsule wake, the flow-field around the parachute is steady, a critical finding. Figure 9 (bottom) is a comparison of the simulated to measured bow at Mach 1.5, 2, and 2.5. The results indicate excellent agreement, within 1.5% of measured values. Similarly, measured drag compares to within 1% of the simulations<sup>26</sup>. These are within the experimental measurement error.

#### E. Canopy with Entry Vehicle Results

The canopy flow field differed markedly from the canopy alone flow field as seen in shadowgraph in Figure 9. The flow field and drag were unsteady and varied in a cyclical fashion. The bow-shock shape and position varied from conical to detached in a periodic fashion. Coincident with this were large fluctuations in measured drag. For example, the *RMS* component of drag varied from 20 to 50% of the mean value from Mach 1.5 to 2.5 (Fig. 10). This compares with <1% for the canopy alone configuration over the same Mach number range. Mach dependence of the flow field was also apparent with bow-shock oscillation frequency of 200 and 300 Hz at Mach 1.5 and 2.0 respectively and drag coefficient decreasing with Mach number. The critical finding here is that the capsule wake coupling is the source of the supersonic flow-field instability resulting in drag fluctuation and pressure non-uniformity within the canopy.

Other key experimental observations from the canopy-with-capsule flow field include a reduction in canopy flow field unsteadiness with increasing canopy to capsule size ( $D_o/d$ ). Increasing the trailing distance from an  $x/d$  of 10 to 14 had a less pronounced but similar effect. The experimental results indicate that as the magnitude of the wake is reduced (relative to a fixed parachute size); coupling to the canopy bow-shock is reduced, as is the flow unsteadiness.

The effect of parachute trim was also apparent. At a trim angle of 5-deg, from the free stream direction, the most violent bow-shock oscillation. It appears as though direct impingement of the wake pressure boundary on the canopy leading edge enhances coupling to the bow-shock. At greater than 5 degrees coupling was reduced and at 10 deg trim angle approached that of the canopy alone flow field. Capsule angle of attack was also observed to affect the parachute bow-shock in that its apex was shifted to coincide with the centerline of the wake core. From 0 to 10-deg, however, the basic physics of the interaction was similar.

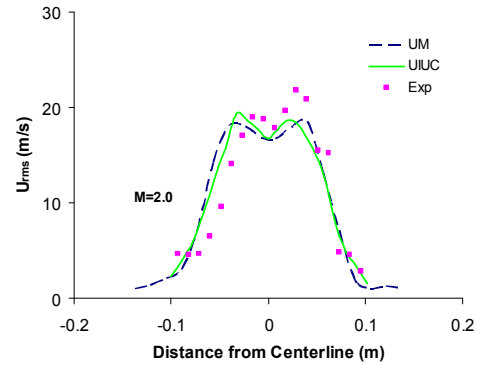


**Fig 8. Comparison of measured and simulated radial wake profiles of *RMS* axial velocity at Mach 2. Data is from the tunnel (capsule) centerline at  $x/d=10$ <sup>26</sup>.**

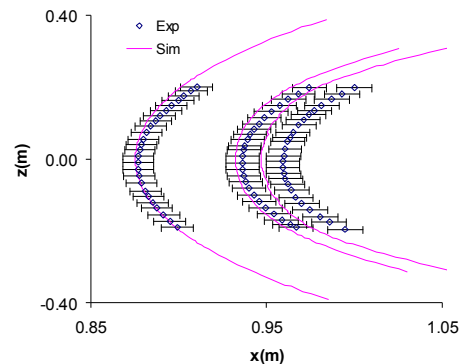
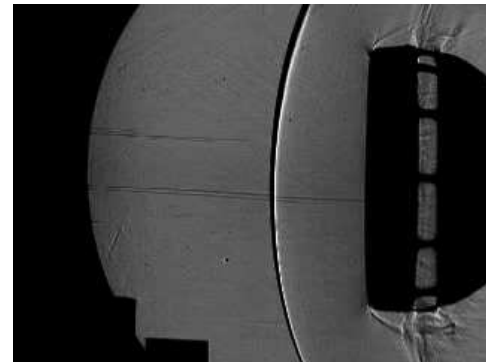


**Fig 9. (Top) Comparison of simulated and measured mean bow-shock position for the canopy alone flow field. (Bottom) Shadowgraph of the canopy alone bow-shock radial wake at Mach 2.0<sup>26</sup>.**

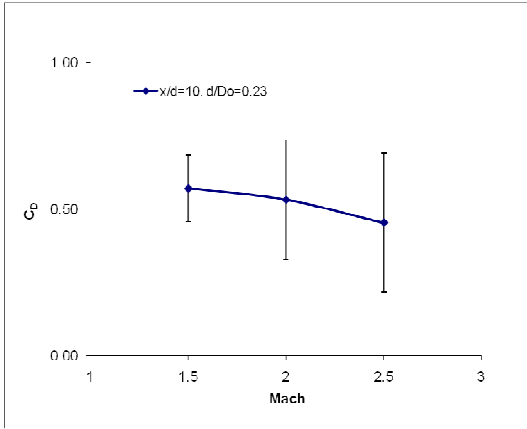


**Fig 10. Mean drag coefficient measurement for the canopy with entry-vehicle configuration with  $x/d=10$  and  $d/D_0=0.23$  (19.7 m parachute). Error bars indicate RMS drag variation with Mach number.**

Comparison of the instantaneous *PIV* and DES computed bow-shock velocity field indicates good agreement in terms of Mach number, shock shape, and wake interaction as shown in Fig. 12. They differ in terms of the axial shock motion where the DES simulation predicts a larger axial excursion than the measured *PIV* data. As the *PIV* data were collected at 5 Hz, it is possible that this excursion was not resolved. As a result it is more accurate to compare the mean shock position for fully qualitative comparison.

## V. Flexible Parachute Experiment

Supersonic wind tunnel tests of 4% scale *MSL* parachutes were conducted in the *GRC 10x10* supersonic wind tunnels. See section IV and reference 29 for details of the tunnel operation. The flexible test program investigated the aerodynamic coupling of the entry-vehicle wake to parachute flow-field and the resultant canopy fabric dynamics. Specifically, the experiment was intended to determine the cause and functional dependence of supersonic area oscillations. Results from the test have been used to determine the frequency of the instability, dynamic drag variation, and provide an update to the Mach efficiency curve for Viking-type *DGB* parachutes from Mach 2.0 to 2.5. The test program has also provided a validation dataset for the fluid-structure interaction computational tools described in section III<sup>26,30</sup>.

A schematic of the test configuration is shown in Fig. 13. The parachute nominal diameter was 0.8m or 4% of flight scale, chosen to provide the maximum size parachute while ensuring that all capsule shock reflections

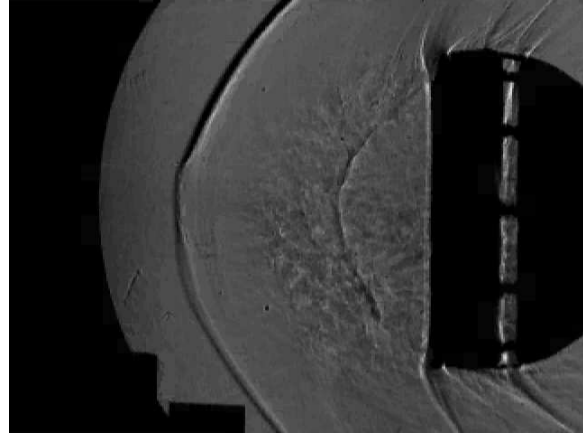


**Fig 11. Shadowgraph of the rigid canopy with entry-vehicle flow field at Mach 2.0,  $d/D_0=0.23$  configuration, and  $x/d=10.9$ .**

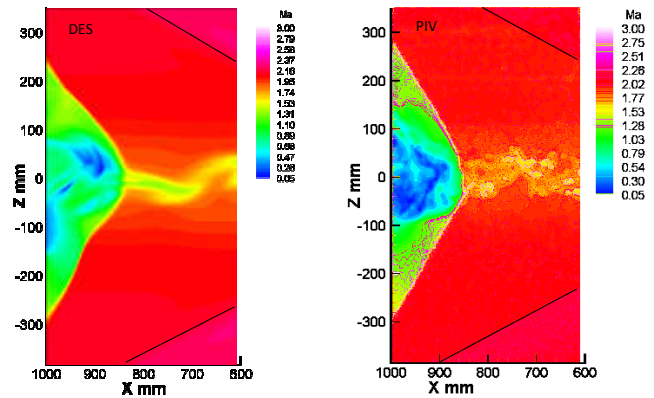


**Fig 12. Comparison of bow-shock region axial instantaneous velocity field for (left) measured *PIV* data and (right) DES simulation at Mach 2.0<sup>28</sup>.**

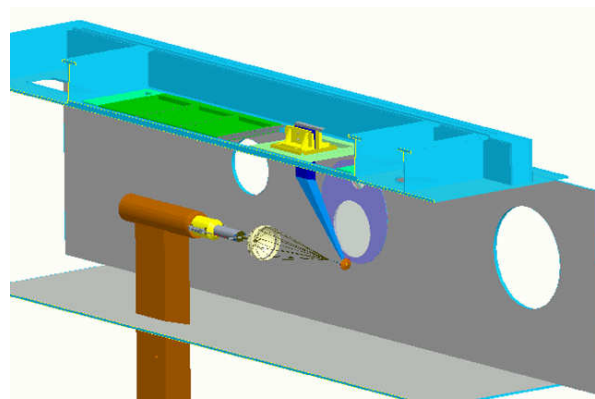


**Fig 13. 4% scale flexible test configuration in the *GRC 10x10* supersonic wind tunnel.**

**Table 2. 4% scale DGB parachute-with-capsule test matrix<sup>31</sup>.**

Test	Mach	High $Q$		Low $Q$		Trim (deg)	$d/D_o$	$D_o$ (m)	$x/d$
		$Re$ ( $\times 10^6$ )	$Q$ (kPa)	$Re$ ( $\times 10^5$ )	$Q$ (kPa)				
Constrained	2	1.0	16.8	2.0	4.3	0	0.21	0.8	10.6
	2.2	1.1	18.3	2.4	3.8				
	2.5	1.2	19.8	2.5	3.1				
Constrained	2	1.0	16.8	2.0	4.3	10	0.21	0.8	10.6
	2.2	1.1	18.3	2.4	3.8				
	2.5	1.2	19.8	2.5	3.1				
Unconstrained	2	1.0	16.8	2.0	4.3	variable	0.21	0.8	10.6
	2.2	1.1	18.3	2.4	3.8				
	2.5	1.2	19.8	2.5	3.1				

occurred downstream of the parachute. A swept-back diamond-wedge stainless steel strut mounted the entry-vehicle (at a zero degree angle of attack), to the tunnel ceiling providing a rigid interface with insignificant vibration during operation. The entry vehicle has a 0.17 m maximum diameter providing a  $d/D_o$  of 0.21 (the scaling for a 21.5 m flight parachute). As with the rigid experiment, the strut was sized to provide minimal aerodynamic interference with sufficient stiffness to prevent capsule vibration when on condition. The parachute was affixed to the entry vehicle via a single axis load cell mounted in the entry-vehicle interior as shown in Fig. 14 (top). The parachute terminates in a Kevlar single riser which was connected to the load cell via a swivel and another textile riser, providing three transverse and three rotation degrees of freedom. The trailing distance obtained by this configuration was 10.6, as measured from the capsule maximum diameter to parachute leading edge.

The test program explored three fundamental configurations: a fixed 0 deg parachute trim angle, a 10 deg trim angle, and the parachute free to trim and cone unconstrained relative to the entry-vehicle. The constrained parachute configuration was maintained at a fixed angle with respect to the entry-vehicle by a constraining rod that passed through the apex of the parachute and connected to the internal tunnel balance mount / translation stage as shown in Fig. 14 (bottom). The constrained parachutes were fitted with a vent ring into which the suspension lines terminated in the canopy apex<sup>31</sup>. The ring allowed the parachute to freely translate and rotate over the constraining rod, but prohibited transverse motion. Vent blockage due to the rod was accounted for by increasing the size of the vent. The balance mount can be configured to provide up to a 20-deg angle relative to the free-stream direction. The unconstrained configuration had the constraining rod removed from the balance mount allowing it to trim and cone in a flight-like manner. The unconstrained parachutes also had no vent ring with and continuous suspension lines fed through the apex, similar to the flight construction. In both cases the capsule was maintained at a zero degree angle of attack relative to the flow field. See 32 reference for more detail on the test configuration. The test matrix for the flexible experiment is shown in Table 2. As simulations suggested area oscillations are turbulence dependent, test conditions were chosen to match the Mach and Reynolds numbers of the MSL deployment envelope, resulting in substantially higher dynamic pressures ( $Q \sim 20$  kPa) than flight<sup>30,33</sup>. These tests are referred to as “High”  $Q$  in the test matrix. “Low”  $Q$  runs ( $Q \sim 4$  kPa) were also included in the test matrix, to investigate a more flight like dynamic pressure, determine Reynolds number dependence to the parachute-wake coupling, and increase parachute lifetime to enable PIV measurement.

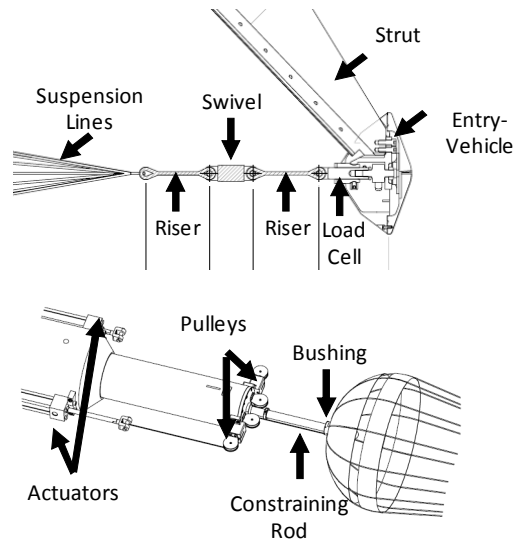


**Fig 14. (Top) Parachute to capsule connection and (bottom) constrained parachute configuration<sup>31</sup>.**

The parachute test articles were similar in construction and design to the flight articles with differences related to the high dynamic pressure environment and the small scale. Differences include fewer gores (24 versus 80), heavier grade nylon fabric, and proportionately thicker Kevlar suspension lines. This is unavoidable but material strains are expected to be within the linear elastic limit for both. The material scaling differences increased the stiffness of the subscale articles, relative to full-scale, but the effect on the parachute's response is believed to be second order. Thicker suspension lines were found to have the most influence due to aerodynamic interaction with the upstream parachute flow field. As a result, proportionate to flight scale thickness suspension line parachutes were fabricated for the low  $Q$  runs to investigate the effect of suspension line interference and improve *PIV* data quality. More details on the parachute construction can be found in reference34.

Deployment of the parachute in the subsonic start up and supersonic environment was found to be a significant challenge in the implementation of the test program. A Spectra deployment sleeve approach with an actively controlled pneumatic tensioning system was selected to minimize relative motion and protect fabric from friction burning and self-abrasion prior to deployment. The sleeve utilized a break-tied daisy chain chord to de-lace the sleeve upon command of an actuator. More details can be found in reference 34.

Similar to the rigid test, non-intrusive diagnostics were chosen to minimize interference with the wake structure and its interaction with the parachute flow-field. Shadowgraph of the parachute bow-shock region was obtained through optical windows on either side of the test article (Fig. 13). Images were collected at 2000 to 4000 fps to resolve the frequency and of the parachute bow-shock oscillation and in some instances capture the supersonic inflation. High speed video was collected through four camera views, needed to compute the fabric shape data through photogrammetric reconstruction. Axial force was measured with a single-axis load cell mounted within the capsule. The parachute force was transmitted to the load cell via a textile member (single riser), swivel, and universal joint. Data were collected at 20 kHz. Particle image velocimetry was also used to compute parachute bow-shock region flow field three-component velocity and turbulent statistics. The *PIV* implementation for the flexible test was identical to that described in section IV for the *GRC* facility in terms of camera placement, sampling frequency (5Hz) and spatial resolution (2 mm). As the *PIV* technique requires several hundred instances (or several minutes of parachute flight) for statistical sampling of the flow field, *PIV* was only used during the low dynamic pressures runs. The high dynamic pressure canopy lifetime was too short to yield useful *PIV* data from a statistical sense and was not attempted. More detail on the optical access can be

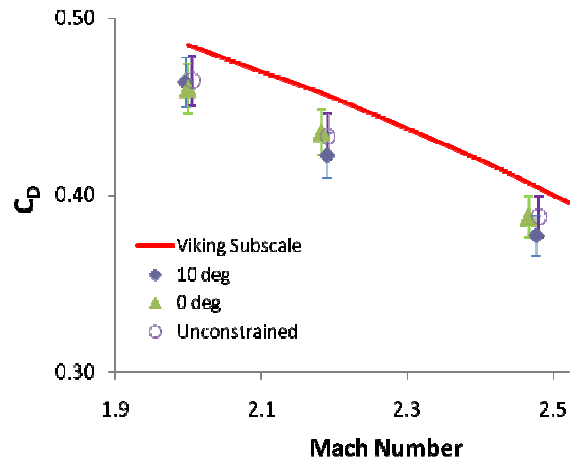


Fig 15. Mean drag coefficient measurements of a 0.8m *DGB* parachute in the *GRC* 10x10 wind tunnel test program compared with Viking era data<sup>25,31</sup>. Error bars indicate experimental measurement error

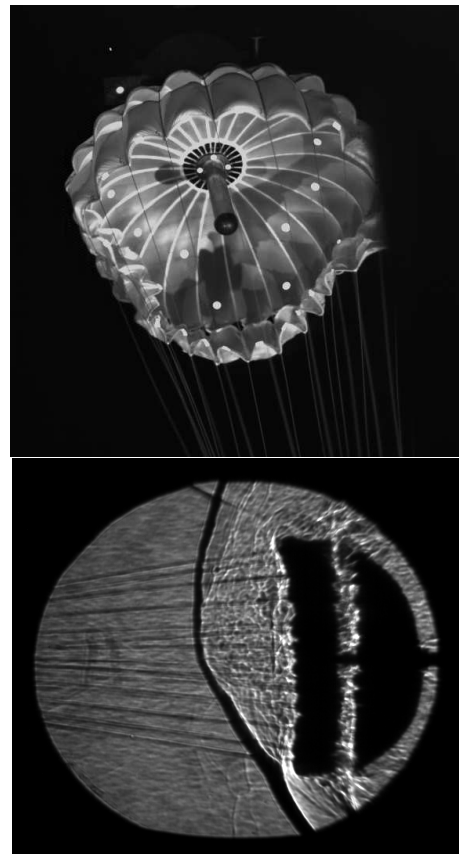


Fig 16. 0.8 m *DGB* parachute (top) high speed video and (bottom) shadowgraph images at Mach 2 as tested in the *GRC* 10x10 supersonic wind tunnel during an area oscillation event.

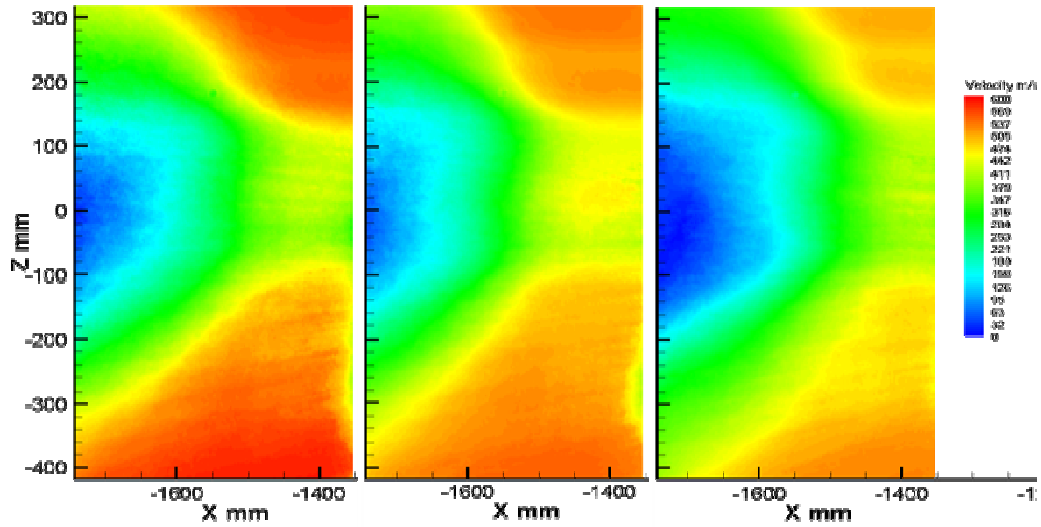


Fig 17. *PIV* measurement of mean velocity magnitude in the parachute bow-shock for the unconstrained 0.8 m *DGB* parachute at Mach 2.5, 2.2, and 2.0 (left to right).

found in reference 31.

## A. Experimental Results

The experimental results for the flexible test include description of the canopy motion and fabric dynamics from parachute drag (normal force), high-speed video, Shadowgraph of the parachute flow-field, and *PIV*. Photogrammetric data reduction is in process and will be presented in a future publication.

The measured axial or normal force was used to compute the drag coefficient. The drag coefficient versus Mach number is plotted in Fig. 15 for the high  $Q$  unconstrained runs from Mach 2 to 2.5 (see reference 35 for the remaining data sets). Plotted alongside the *MSL* data are Viking era subscale test drag coefficient measurements. The datasets compare to within the measurement error of the load cell<sup>25</sup>. Both datasets indicated a trend of decreasing  $C_D$  with Mach number. It should be noted that any side force experienced in this configuration is not included in this calculation of drag as the load cell was single-axis.

Figure 16 (top) shows the partially collapsed canopy at Mach 2.2 operation, illustrating an area oscillation event. Prior to the onset of an area oscillation the parachute fabric dynamics are limited to periodic with in-folds in the band region. During an oscillation, however, the band in-fold was more extreme and propagated inward towards the disk or center of the canopy. The resultant projected area variation ranged from 40 to 70% from Mach 2 to 2.5 respectively. The resultant frequency of the area oscillation event was 70 to 90 Hz, increasing with Mach number. It is important to note that area oscillations did not occur throughout the constant Mach number flight, instead their insert appeared to be random; however once initiated they were followed for 3 to 5 additional oscillations,. Suspension line shocks were also observed to exacerbate the oscillation by disrupting the bow-shock. During the low  $Q$  runs the canopy dynamics were found to be less severe consistent with reduced wake turbulence and suspension, consistent with the Reynolds number dependence of the flow field.

Shadowgraph data provided unique insight into the flow field. Shadowgraph video clearly indicates that the pressurization and depressurization of the parachute were driven by the changing morphology and stand-off distance of the parachute bow-shock (Fig. 16 bottom). The periodic variation in the flow-field was similar to that of the rigid parachute experiments described in section IV, confirming the aerodynamic nature of this phenomenon. Shadowgraph data also revealed the effect of suspension line aerodynamic interaction with the flow-field. Shocks from the suspension lines, in certain instances, appeared to disrupt the parachute bow-shock. Also, as will be discussed in the context of the *PIV*, the bow-shock appeared to creep up the suspension lines. Area oscillation events did not require a suspension line induced disruption to experience significant band in-folding. However, suspension line shock generation seemed to exacerbate the canopy dynamics. The Shadowgraph data also indicate asymmetry in

the bow-shock due to the strut and canopy trim. A pressure discontinuity was also observed at the canopy mouth, similar to that measured in the rigid experiment. The source of this discontinuity may be related to an inflow / outflow boundary at the stagnation point.

Instantaneous *PIV* flow field data were collected and averaged. Figure 17 indicates the mean axial velocity field in the parachute bow-shock region at Mach 2.0, 2.2 and 2.5 for the unconstrained, low  $Q$  case. The effect of wake coupling and suspension line interaction is evident in the *PIV* measurements. The oblique shock angle is also evident with the most conical shock at Mach 2.5. The apparent blur of the image is due to the ensemble averaging of the canopy as it trims and cones about the *PIV* data plane. The constrained data sets resulted in more refined bow-shock profiles. Although not shown, *PIV* also resolved the apparent creep of the bow-shock up the suspension lines. It is unclear if it is this upstream motion, the suspension line shocks, or a combination of these effects that further exacerbate area oscillations. But the reduction in suspension line cross sectional area will reduce this effect, which has important implications of *MSL* versus the Viking era parachute.

## VI. Discussion

The data collected and computational tools developed as part of the *MSL* supersonic qualification program have led to significant insight into the supersonic operation of *DGB* parachutes. The primary findings from the program are summarized below in terms of capsule wake, parachute size, Mach,  $Re$ , suspension line interaction, and supersonic inflation.

### A. Capsule Wake Effect

The canopy alone and canopy with capsule rigid experimental configurations clearly indicated the effect of the wake coupling to the parachute's bow-shock. In the absence of the wake, bow-shock and drag were steady with *RMS* fluctuation less than 1% of the mean. When the wake was introduced the bow-shock shape and standoff distance exhibited an oscillatory motion, manifesting as large fluctuations in drag. In the limit of a large trailing distance or large parachute relative to entry-vehicle diameter, the coupling is reduced and the flow-field becomes more stable.

### B. Parachute Size

The rigid parachute experiment explored the effect of parachute size via the parameter  $d/D_0$ . Consistent with the finding that the entry-vehicle wake was the source of the flow field unsteadiness, and increase in the relative size of the wake to the canopy size, tended to increase the flow field unsteadiness. Similarly, increased trailing distance tended to reduce the coupling to the wake and resultant unsteadiness. The critical find here is that the flow physics associated with a 19.7, 23, and 25 m parachute is continuous and intuitive.

### C. Mach and $Re$ Dependence

Mach dependence was readily observed in the rigid and flexible parachute experiments. Increase in Mach tended to increase coupling between the wake and bow-shock and resulted in drag reduction and large *RMS* variation in flow field parameters, and more unstable flight in terms of parachute trim and coning. Canopy fabric dynamics were also found to be exacerbated with higher Mach number in term so of area oscillation frequency and project area variation. Reynolds number effects were evident from the comparison of the low and high  $Q$  runs. The low  $Q$  runs, although at the same Mach, were not as unsteady with parachute motion and oscillations less severe. The important finding here is that when designing a subscale test, Reynolds number effects must be evaluated as turbulence plays a major role in the supersonic fluid structure interaction.

### D. Suspension Line Interaction

A critical finding of the flexible parachute experiment was the effect that suspension line aerodynamic interaction has on the flow-field unsteadiness. The rigid experiment could not address this feature. Shadowgraph data indicated that shocks emanating from the suspension lines, in conjunction with wake to bow-shock coupling were responsible for the area oscillation event. Close inspection of the high speed and shadowgraph video indicated

that although each oscillation was induced by the bow-shock oscillation, the whole scale disruption of the shock was related to the suspension line aerodynamic interaction. It is fair to say that the suspension line interaction resulted in exacerbated canopy depressurization and larger projected area reduction. Important to note is the fact that the Viking era Dacron suspension lines were six times thicker than modern day Kevlar suspension lines suggesting that suspension line interaction will be reduced for *MSL* versus a Viking era parachute of the same approximate size/load.

## E. Supersonic Inflation

High-speed video was used to document the supersonic initial inflation, yielding some of the first images of that process at this Mach number regime. Although a sleeve deployment differs from a mortar deploy (no bag stripping forces), there is qualitative similarity in the initial presentation of the canopy leading edge to the free-stream and the canopy filling that ensues. The inflation times ranged from 9 to 15 ms and appeared similar for all the case investigated. An interesting feature in the inflation characteristics of all runs was the presence of a multi-gore in-fold, a presentation consistent with the *PEPP* 19.7 parachute inflation<sup>11</sup>. Another interesting feature was the similarity between the canopy presentation midway into the inflation and the area oscillation event. In terms of canopy dynamics, flag-drag, flapping, and area oscillation were not evident during the inflation process.

## VII. Conclusion

The *MSL* parachute supersonic qualification program was implemented to address the large scale, high Mach deployment, and propensity for area oscillations to occur at the anticipated flight deployment conditions. Through a combination of subscale testing and computational simulations the aerodynamics of the supersonic operation of *DGB* chutes has been ascertained. The program has explored the functional dependence of Mach number, Reynolds number, geometric scale, and dynamic pressure on this supersonic instability. The rigid experiments and corresponding simulations indicate the coupling between the entry-vehicle wake and bow-shock results in a pressurization and depressurization of the canopy flow-field consistent with the transition from a conical to detached shock resulting in large drag fluctuations and flow unsteadiness. Configurations investigating parachute sizes of 19.7, 23, and 25 m indicate the flow-physics is continuous and essentially unchanged. In the absence of an entry-vehicle the parachute flow field and resultant drag performance is steady. Detailed qualitative comparisons between drag and velocity in the wake and upstream canopy flow-field indicate excellent agreement between experiment and simulation. The flexible parachute experiments yielded new insight into the fluid structure interaction of the *DGB* parachute and entry-vehicle wake. The bow-shock variation was very similar to that of the rigid experiment and also revealed that area oscillations are a result of the bow-shock shape change and suspension line interaction. Particle Image Velocimetry was demonstrated for the first time on a parachute in supersonic flow, yielding time and spatially accurate measurements of flow velocity and turbulent statistics ideal for validation simulations. *PIV* has provided quantitative measurement of the bow-shock interaction, wake closure, and turbulent statistics for the rigid and flexible configurations. *CFD* validation simulations exhibit excellent agreement with the experimental data collected. *FSI* validation simulations are currently underway.

Drag measurements revealed that parachute drag is consistent with prior Viking era measurements. Therefore, changes to the existing *MSL* Mach efficiency curve are not required. High speed video indicates that fabric dynamics for the unconstrained parachute are primarily limited to in-folding in the band region with larger in-folds creating the area oscillation event. The results suggest that non-dimensional aerodynamics parameters and geometric scaling are valid in understanding the physics of supersonic parachute operation in the regime of interest to *MSL*.

## Acknowledgments

The authors would like to acknowledge James Roeder, Mark Wernet, Adam Wroblewski, Randy Locke, Rick Kelsch, Lance Foster, and Christine Pastor of *NASA GRC*, James Heineck, James Bell, Ed Schairer of *NASA Ames*, and Tom Jones of *NASA Langley*, for their development and conduct of the rigid and flexible parachute test programs. The authors would also like to acknowledge Professor William Garrard, Dr. Michael Barnhardt and Vladimir Gizzak of the University of Minnesota, Professor Fehmi Cirak of the University of Cambridge, and Professor Keith Stein of Bethel University, for their development of the computational simulations and assistance

with design of experiments. The Jet Propulsion Laboratory, California Institute of Technology carried out the activities described in this paper, under a contract with the National Aeronautics and Space Administration. Copyright 2009. All rights reserved.

## References

- <sup>1</sup> D. Way, R. Powell, A. Chen, and A. Steltzner, "Asymptotic Parachute Performance Sensitivity" 2006 IEEE Aerospace Conference, Big Sky, MT, March 2006.
- <sup>2</sup> R. Mitcheltree, W. Lee, A. Steltzner, and A. SanMartin, "Mars Exploration Rover Mission: Entry, Descent, and Landing System Validation," IAF Paper IAC-04-Q.3.a.02, October, 2004
- <sup>3</sup> P. Hoffman, T. Rivellini, E. Slimko, N. Dahya, A. Agajanian, J. Knight, A. Sengupta, B. Thoma, R. Webster, J. Gallon, M. Gradziel, "Preliminary Design of the Cruise, Entry, Descent, and Landing Mechanical Subsystem for *MSL*," IEEE Aerospace Conference, March 3-10, 2007, Big Sky, MT.
- <sup>4</sup> R. Mitcheltree, A. Steltzner, A. Chen, M. SanMartin, and T. Rivellini "Mars Science Laboratory Entry Descent and Landing System Verification and Validation Program," IEEE- 0-7803-9546-8/06.
- <sup>5</sup> A. Steltzner, D. Kipp, A. Chen, P. Burkhart, C. Guernsey, G. Mendeck, R. Mitcheltree, R. Powell, T. Rivellini, M. San Martin, D. Way, "Mars Science Laboratory Entry, Descent, and Landing System", IEEAC #1497, IEEE Aerospace Conference, March 4-11, 2006, Big Sky, MT.
- <sup>6</sup> R. Ingoldby et. al., "Entry Data Analysis for Viking Landers," Feb 2002, Contractor Report (1976).
- <sup>7</sup> D. Dickenson et. al., "Balloon Launched Decelerator Test Post-Flight Test Report *BLDT* Vehicle AV1," TR-3720289, Sept 1972.
- <sup>8</sup> D. Dickenson et. al., "Balloon Launched Decelerator Test Post-Flight Test Report *BLDT* Vehicle AV4," TR-3720295, Oct 1972.
- <sup>9</sup> R.D. Moog and F.C. Michel, "*BLDT* Summary Report," TR-372039, March 1973.
- <sup>10</sup> A. Sengupta, A. Steltzner, A. Witkowski, and J. Rowan, "An Overview of the Mars Science Laboratory Parachute Decelerator System," IEEE-1432-2007, March 2007.
- <sup>11</sup> H. Murrow and J. Mcfall, "Some Test Results from the *NASA* Planetary Entry Parachute Program," *J. Spacecraft*, Vol. 6 (5): 621-623, 1969.
- <sup>12</sup> D.E Reichenau., "Aerodynamic Characteristics of Disk-Gap-Band Parachutes in the Wake of Viking Entry Forebodies at Mach Numbers from 0.2 to 2.6," AEDC-TR-72-78, Arnold AFB, Tennessee, (1972).
- <sup>13</sup> L. Couch, "Drag and Stability Characteristics of a Variety of Reefed and Un-Reefed Parachute Configurations at Mach 1.8 with an Empirical Correlation for Supersonic Mach numbers," *NASA* TR R-429, February 1975.
- <sup>14</sup> I. Nompelis et. al., "A Parallel Unstructured Implicit Solver for Hypersonic Reacting Flow Simulation," AIAA 2005-4867.
- <sup>15</sup> M. Wright, D. Bose and G.V. Candler, "A Data-Parallel Line-Relaxation Method for the Navier-Stokes Equations," AIAA Journal, Vol. 36, No.9, pp. 1603-1609, Sept. 1998.
- <sup>16</sup> Barnhardt, M., T.W. Drayna, I. Nompelis, G.V. Candler, and W.L. Garrard, "Detached Eddy Simulations of the *MSL* Parachute at Supersonic Conditions," AIAA Paper 2007-2529, May 2007.
- <sup>17</sup> C. Pantano, R. Deiterding, D. J. Hill, and D. I. Pullin. "A low-numerical dissipation patch based adaptive mesh refinement method for large-eddy simulation of compressible flows" *J. Comput. Phys.*, 2006.
- <sup>18</sup> R. Deiterding, R. Radovitzky, S.P. Mauch, L. Noels, J.C. Cummings and D.I. Meiron. A virtual test facility for the efficient simulation of solid materials under high-energy shock-wave loading. *Engineering with Computers*, 22(3-4): 325-347, 2006.
- <sup>19</sup> A. Sengupta et. al., "Overview of the Supersonic Qualification Program for the Mars Science Laboratory Parachute Decelerator System," AIAA-2007-2542, Presented at the 19th AIAA Aerodynamic Decelerator Systems Conference, Williamsburg, VA, May 21-24 2007.
- <sup>20</sup> K Stein, et. al, "Parachute Fluid-Structure Interactions: 3-D Computation," *Computer Methods Appl Mech Eng* 190 (2000) 383-386. *AIAA J* 38 (2000) 139-146.
- <sup>21</sup> K Stein, et. al, "Parachute Fluid-Structure Interactions: 3-D Computation," *Computer Methods Appl Mech Eng* 190 (2000) 383-386.
- <sup>22</sup> F. Cirak and M. Ortiz. "Fully C1-conforming subdivision elements for finite deformation thin-shell analysis," *Int. J. Numer. Meth. Engineering*, 51:813-833, 2001.
- <sup>23</sup> F. Cirak and R. Radovitzky, "A Lagrangian-Eulerian Shell-Fluid on Level Sets," *Computers & Structures*, 83:491-498, 2005.
- <sup>24</sup> R. P. Fedkiw, "Coupling an Eulerian fluid calculation to a Lagrangian solid calculation with

---

the ghost fluid method,” J. Comput. Phys. 175:200–224, 2002.

<sup>25</sup> I. Jaremenko, S. Steinberg, and R. Faye-Petersen, “Scale Model Test Results of the Viking Parachute System at Mach Numbers from 0.1 Through 2.6,” TR-3720181, November 1971.

<sup>26</sup> A. Sengupta et. al., “Results from the Mars Science Laboratory Parachute Decelerator System Supersonic Qualification Program,” IEEE-1435-2008, March 2008.

<sup>27</sup> A. Ruge, “Torque Measuring Apparatus,” US Patent # 2392293, Jan 1946.

<sup>28</sup> M. Wernet et. al., “Application of Stereo *PIV* on a Supersonic Parachute Model,” AIAA-0070-2009, Presented at the 47<sup>th</sup> AIAA Aerospace Sciences Conference, Orlando, FL Jan 2009.

<sup>29</sup> <http://facilities.GRC.NASA.gov/documents/TOPS/Top10x10.pdf> , “10- by 10-Foot Supersonic Wind Tunnel,” TOP3-00226, Jan 2007.

<sup>30</sup> M. Barnhardt, T. Drayna, Ioannis Nompelis, G.V. Candler, and W. Garrard, “Detached Eddy Simulations of the *MSL* Parachute at Supersonic Conditions,” AIAA-2529-2007, May 2007.

<sup>31</sup> A. Sengupta et. al., “Supersonic Disk Gap Band Parachute Performance in the Wake of a Viking-Type Entry Vehicle from Mach 2 to 2.5,” AIAA-2008-6217, Presented at the AIAA Atmospheric Flight Mechanics Conference, Honolulu, HI, Aug 18-21 2008.

<sup>32</sup> A. Sengupta et. al., “Supersonic Testing of 0.8 m Disk Gap Band Parachutes in the Wake of a Subscale *MSL* Entry Vehicle” 20th AIAA Aerodynamic Decelerator Conference, Seattle, WA May 4-8th 2009.

<sup>33</sup> V. Gidzak et. al., “Simulation of Fluid-Structure Interaction of the Mars Science Laboratory Parachute,” AIAA 2008-6910, August 2008.

<sup>34</sup> A. Witkowski, M. Kandis, J. Reuter and W. Machalick, R. Kelsch, “Design of Subscale Parachute Models for *MSL* Supersonic Wind Tunnel Testing,” AIAA-2009-2999, May 2009.

<sup>35</sup> A. Sengupta et. al., “Supersonic Qualification Program for the Mars Science Laboratory Parachute System” 20th AIAA Aerodynamic Decelerator Conference, Seattle, WA May 4-8th 2009.